LAWRENCE
LIVERMORE
NATIONAL
LABORATORY

LLNL-CONF-438834

Implementation of Pulsed Power Diagnostics on Explosive Flux Compression Generators at LLNL

D. A. Goerz, R. A. Anderson, A. D. White,
J. B. Javedani, D. B. Reisman, T. J. Ferriera,
E. V. Baluyot, R. D. Speer, and D. P. Milhous

June 28, 2010

The 13th International Conference on Megagauss Magnetic Field Generation and Related Topics
Suzhou, China
July 6, 2010 through July 10, 2010

Implementation of Pulsed Power Diagnostics on Explosive Flux Compression Generators at LLNL

D. A. Goerz, R. A. Anderson, A. D. White, J. B. Javedani, D. B. Reisman,
T. J. Ferriera, E. V. Baluyot, R. D. Speer, and D. P. Milhous
Lawrence Livermore National Laboratory
Livermore, CA 94550 USA
Email: <goerz1@llnl.gov>

ABSTRACT

LLNL has developed a family of advanced magnetic flux compression generators used to perform high energy density physics experiments and material science studies. Our high gain advanced helical generator (AHG) can produce currents of 20 MA and energies of 20 MJ. Our ring-lit coaxial generator, when driven by the AHG, can deliver 100 MA currents and over 60 MJ energies to experimental loads. Accurately measuring the performance of these explosive pulsed power devices is important in their development and application. We have incorporated the usual pulsed power diagnostics into our FCGs and experimental apparatus, including Rogowski coils, B-dot probes, and Faraday rotation optical fiber sensors. In addition, we utilize external magnetic and electric field sensors to monitor emissions that can indicate loss mechanisms and fault conditions. The methods for implementing these various diagnostics follow an established practice at LLNL for handling grounding, shielding, and isolation of the multiple stages and auxiliary systems. Sensors are electrically isolated and signal lines are fully enclosed in metallic conduits to provide EMI shielding. Where necessary, electrical signals are converted to optical signals and carried over fibers. All of the high current sensors are custom fabricated, and we perform in-situ calibration using network analyzer equipment to achieve very accurate characterization. This paper describes the details of the sensors, calibration methods, grounding and shielding, and data analysis techniques.

INTRODUCTION

High energy density physics (HEDP) experiments and material science studies are an important part of the scientific research underway at LLNL. High explosive pulsed power (HEPP) is one way to produce extremely high energy density conditions and very high pressures to study material dynamics. Explosively driven magnetic flux compression generators (FCGs) are being developed at LLNL to obtain output currents that far surpass those of large-scale capacitor bank systems. Our near term objective is to measure the equation-of-state and strength properties of materials using sample sizes of 10's of mm^2 with isentropic drives to 10 Mbar.

LLNL has developed a family of advanced magnetic flux compression generators used in explosively driven pulsed power experiments. Our high gain advanced helical generator (AHG) can produce currents of 20 MA and deliver energies of 20MJ [1]. Our ring-lit coaxial generator (CG), when coupled with the AHG, can deliver 100 MA currents and over 60 MJ energies to experimental loads. To date we have conducted four full function tests (FFT) of the combined AHG-CG system while successfully performing HEDP experiments [2]. More details about the AHG-CG system design and the FFT output vacuum power flow design are presented in other papers at this conference [3,4]. LLNL's family of flux compression generators exhibit fast current rise at high-energy levels. A smaller scale flat plate generator (FPG) with similar

features is capable of driving 20 MA of current with a 2-μs exponential rise time. We are now developing a half-scale version of the FFT system called the MiniG that will be capable of delivering currents of 60 MA and energies of 10 MJ with rise times of 2-4 μs.

Accurately measuring the performance of these explosive pulsed power devices is important in their development and application. We have incorporated the usual pulsed power diagnostics into our FCGs and experimental apparatus, including Rogowski coils, B-dot probes, and Faraday rotation optical fiber sensors. In addition, we utilize external magnetic and electric field sensors to monitor emissions that can indicate loss mechanisms and fault conditions.

GROUNDING, SHIELDING AND ISOLATION

In HEDP experiments, it is of the utmost importance to accurately measure current and the uniformity of current distribution at the final stage generator output. However, this is where the conditions that sensors must function in and survive are most extreme. Early in our planning for HEPP testing we developed an approach for grounding, shielding and isolation of the multi-stage pulsed power system that would provide the best opportunity to obtain very high quality data at the output. We chose to provide our experiment ground reference at the load interface flange, and isolate all other parts of the system from ground during operation. This impacted how all the subsystems were developed and implemented. Figure 1 shows a drawing of a combined helical-coaxial FCG system, pointing out the ground reference at the coaxial generator load end, and depicting the dielectric stand and supports for the helical. Figure 2 shows a photograph of the actual hardware.

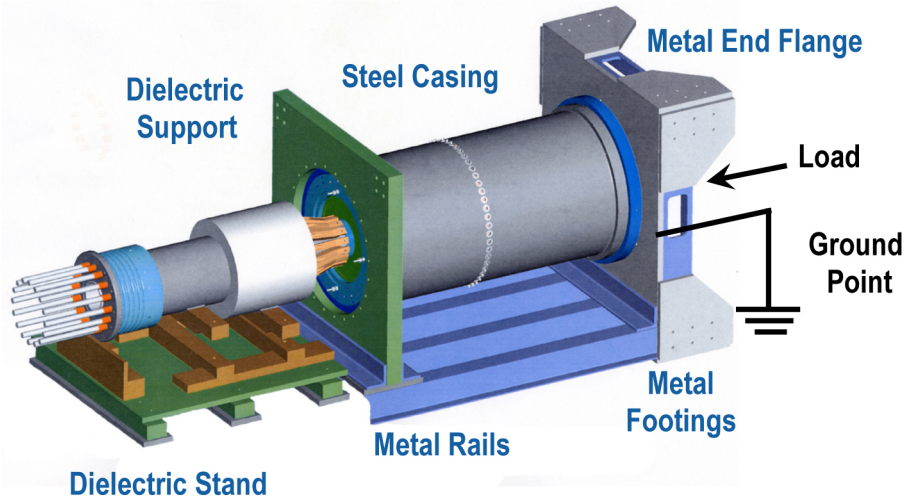

Figure 1. Drawing of helical and coaxial FCGs depicting experiment ground at load end and dielectric stand and support for helical FCG.

To avoid ground loops through subsystems they must be isolated from ground and from each other. The seed bank operates with its output floating with respect to local ground, and is ground referenced to the experiment through its coaxial cable connections. The firesets for both the helical and coaxial generators are isolated from ground and each other. The firesets are custom designed units powered by batteries with pneumatic air controls for safety and fiber-optic controls for charging and firing.

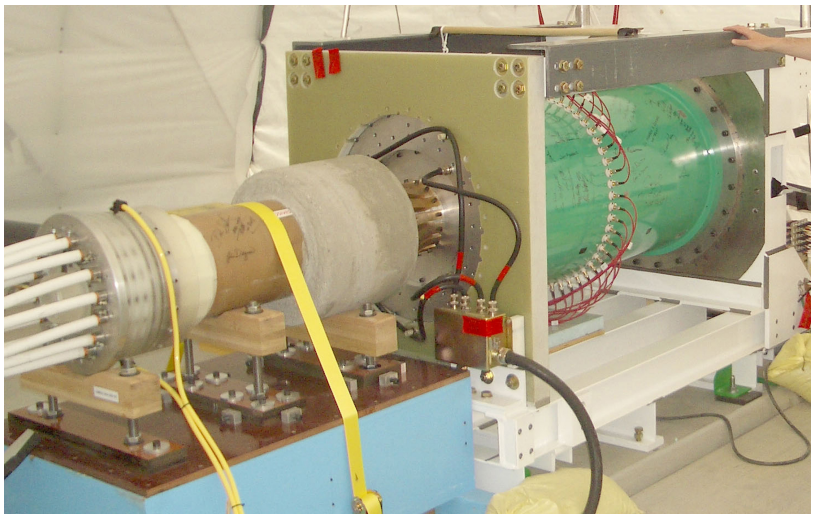

Figure 2. Photo of helical and coaxial FCGs. Support stand for coaxial FCG is made of metal whereas support stand for helical FCG is dielectric.

Figure 3 shows a drawing depicting the isolated fireset and Figure 4a shows a photograph of one. The details of the isolation and operation of these various subsystems are described in other LLNL reports.

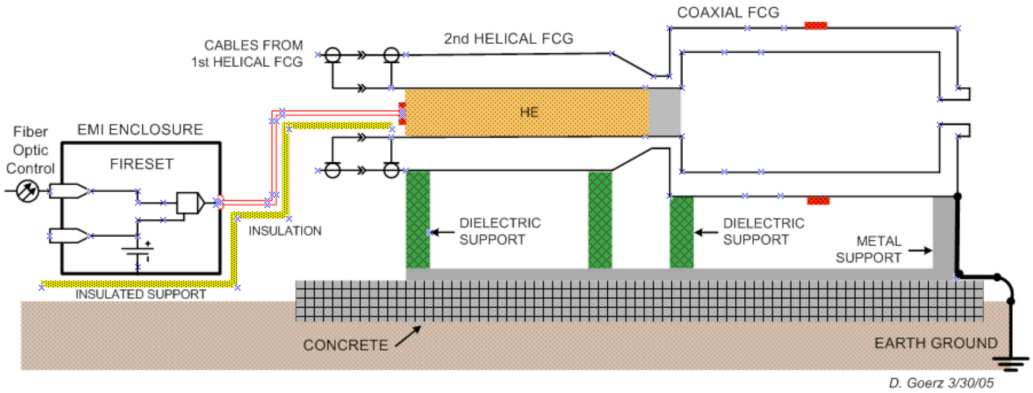

Figure 3. Drawing of implementation of isolation for firesets used in multi-stage FCG system.

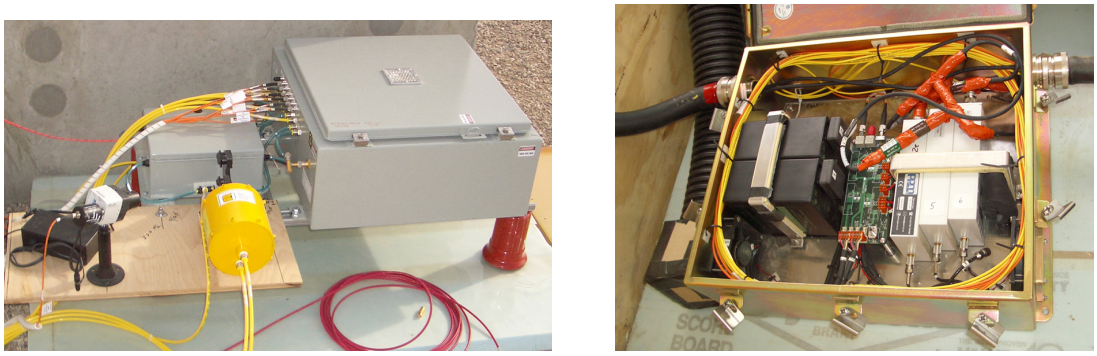

Figure 4. (a) Photo of isolated fireset with pneumatic and fiber optic controls. (b) Photo of battery powered analog fiber-optic data links inside EMI enclosure.

In this paper we focus on the implementation of the pulsed power diagnostics, some of which must also be isolated from ground. For instance, the B-dot sensors that are located at the input of the coaxial generator are kept isolated from ground using analog fiber-optic data links. These analog fiber-optic data links are battery-powered units contained within an EMI-shielded box close to the experiment. Figure 4b shows a photograph of one such unit, while Figure 5 shows a drawing depicting how the isolated analog FO data link is utilized. We have used DC to 10 MHz analog fiber optic links manufactured by PPM [5]. These units actually convert the analog input signals into optical digital signals for transmission over optical fibers.

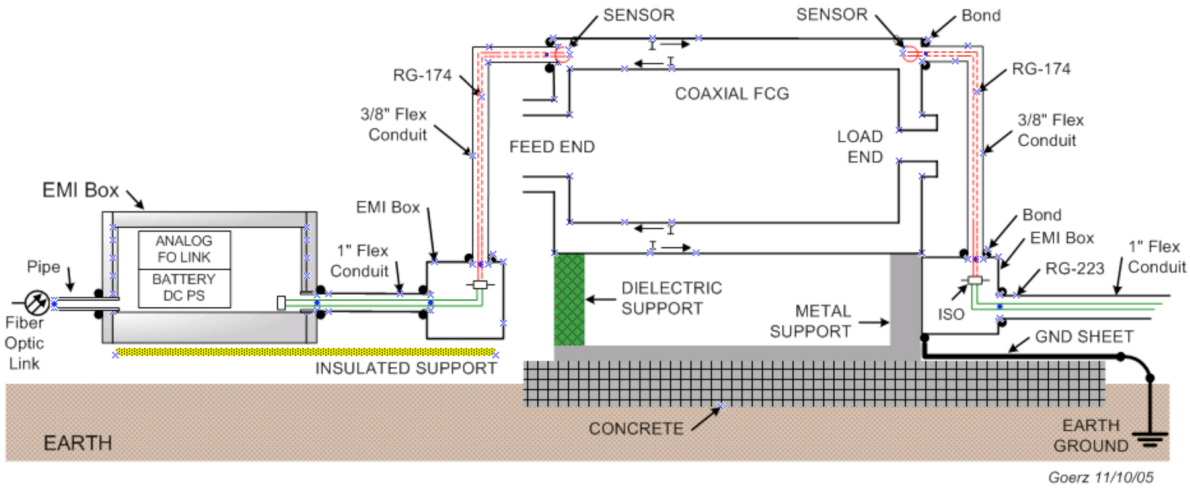

Figure 5. Grounding, shielding and isolation implementation for B-dot sensors at the input and output ends of coaxial FCG. Analog FO links inside the EMI box are shown in Fig. 4b.

SENSORS AND SIGNAL TRANSPORT

Seed bank current monitors

Current viewing transformers (CVTs) are used to monitor the current delivered by the seed bank to the FCG system. Two CVTs are used for redundancy, and both are mounted inside the seed bank enclosure around the current return-path of the seed bank output. Both CVTs are Pearson Electronics Model 1423 [6], which have a sensitivity of approximately 0.5 V/kA into a 50-Ohm termination. The current monitor outputs are attenuated using resistive dividers and then converted into optical signals using analog fiber optic links. At the receiver the signals are converted back into electrical signals, which are recording by digitizers.

Seed bank voltage monitor

A high-voltage monitor is used to record the voltage at the seed bank output during experiment. The high-voltage monitor is a North Star PVM-5-2 [7], which is a resistive and capacitive divider with a sensitivity of approximately 0.5 volts per kilovolt. The probe output is coupled via a calibrated coaxial cable into a high impedance analog fiber optic link, which sends the optical signal over fiber to a receiver chassis in the bunker using the same approach as the seed bank current viewing transformers.

Fireset output current monitor

A Rogowski coil installed at the output of the multi-point fireset is used to monitor the fireset output current during experiment. The Rogowski coil produces a voltage proportional to the time-derivative of the current passing through the load ring. The sensitivity of the Rogowski coil is approximately 64.5E-12 volts per ampere per second into a 50-Ohm termination. The Rogowski coil uses the same type of fiber optic links used for the seed bank voltage and current monitors to couple the signal to recording digitizers in the bunker. In order to maximize the limited dynamic range of the fiber optic link, the Rogowski coil output is filtered using a RC partial-integrator with a time constant of approximately 1.45 microseconds. The filtered output is coupled into the fiber optic link. Numerical correction is applied to the partially integrated data to produce a waveform that is representative of fireset current [8]. The Rogowski data is used to validate fireset performance during the experiment, and provide information regarding detonator burst time and current.

Fireset burst detectors

To monitor fireset function and timing we employ so-called burst detectors developed at LLNL. They are connected in line with the coaxial cables feeding selected detonators, and contain resistive dividers to electro-optic transmitters. When the exploding bridge wire (EBW) bursts, a sizeable (IdL/dt+IR) voltage is developed across the EBW, which the resistive divider senses and applies to the fiber-optic transmitter. The optical signal is carried over fiber to an optoelectronic receiver in the bunker where the electrical signal is recorded by digitizers.

CG B-dot sensors

We designed B-dot sensors to incorporate into both ends of the coaxial generator that would enable us to also provide significant EMI shielding. The details of sensor construction are shown in Figure 6. The B-dot sensors are single-polarity multi-turn loops, formed by wrapping insulated 0.254-mm diameter copper wire around a 1.83-mm plastic mandrel. The copper wire from the loop is twisted to form a twisted pair transmission line. Both the loops and twisted pair are inserted into 4-mm OD quartz tubes, which are then filled with epoxy. The twisted pair leads at the output are soldered to SSMA connectors, which are coupled to coaxial cables within flexible EMI conduit.

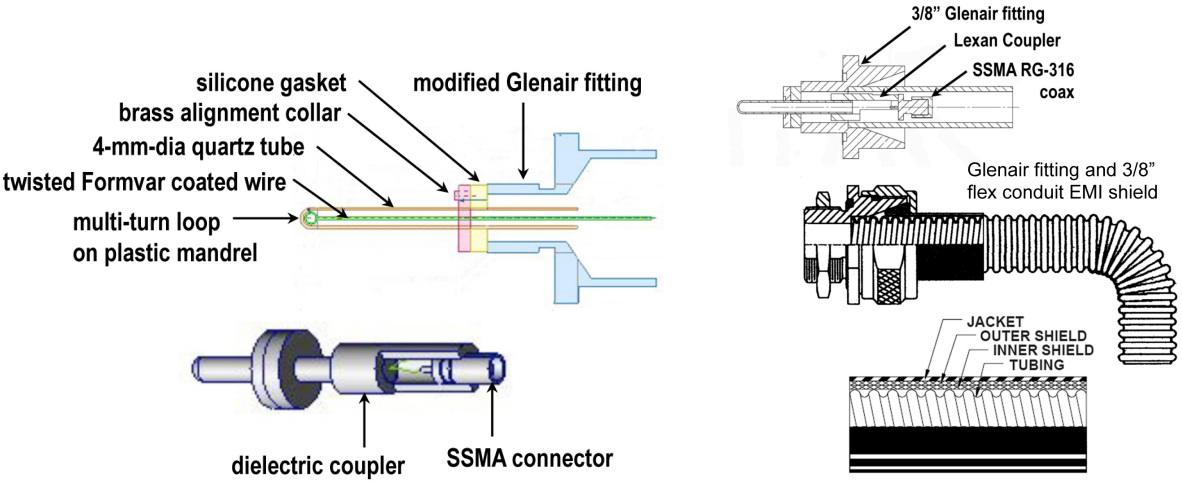

Figure 6. Details of B-dot sensor fabrication (left) and EMI shielding (right).

CG Input B-dot sensors

Four B-dot sensors installed at the coaxial generator input are used to monitor AHG performance. For EMI shielding we incorporated Glenair series-74 helical convoluted tubing [9]. The four sensors are installed at 90° azimuthal intervals at a radius of 23.9 cm. The routing of the flexible conduits to an EMI box can be seen in Figure 2 and is also depicted in Figure 5. Since the B-dot loops are single-polarity and yield differential measurements, we use alternating positive and negative polarity probes, and numerically subtract the common-mode signal from the measured waveforms. Since the probes respond to the time-derivative of the magnetic field, the common-mode rejected outputs are numerically integrated to produce AHG current. Typical sensitivities for the CG input probes are approximately 15 Volts per mega-Ampere per microsecond. The bandwidth of these B-dots greatly exceeds the bandwidth of the AHG I-dot, which is limited to tens of kilohertz.

As mentioned earlier, to prevent significant currents flowing on conduit shields from ground loops, the EMI conduit for the CG input B-dots are isolated from those for the CG output B-dots. This is achieved by connecting them to an isolated EMI box a short distance from the generator. Within the EMI box, shown in Figure 4b, the signals are attenuated, and coupled onto PPM fiber optic links, which carry the signals over fibers to recording digitizers in the bunker.

CG Output B-dot sensors

At the output end of the coaxial generator we have a total of ten B-dot sensors installed at two different radial locations. Six B-dots are installed at the outermost radius of 23.5 cm in the SF6 filled region upstream of the high voltage vacuum insulator. Four B-dots are installed in the vacuum region, at a generator radius of 13.3 cm.

The construction of the CG output B-dots closely resemble that of the CG input B-dots. However, the number of turns is varied according to the desired range of I-dot coverage. Like the CG input B-dot probes, the CG output B-dot probes are installed in opposite-polarity pairs to facilitate numerical common-mode rejection using the recorded waveforms.

Early on in our experimental campaign we had some of the output B-dot signals go to isolated analog fiber-optic links and other B-dot signals carried on cables all the way to digitizers in the bunker. The EMI shielding of B-dot sensors and cables for this arrangement is depicted in Figure 7.

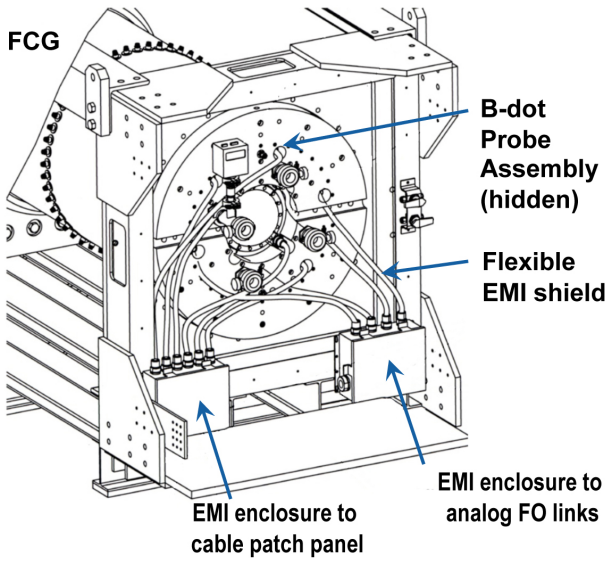

Figure 7. Drawing of FCG output end showing EMI shielding of B-dot sensors and cables.

Since our first successful full function test, which proved out our EMI shielding approach, we have forgone the analog fiber-optic links at the CG output, and relied exclusively on the Faraday cage approach discussed later.

CG Output Faraday rotation fiber sensors

Two fiber-optic sensors are installed inside the coaxial generator to monitor output current using the Faraday rotation method [10]. The sensors are formed from twisted single-mode fiber wrapped approximately one time around the HV vacuum insulator. Figure 8 shows the location and routing of the fibers. The sensors, associated hardware and data reduction techniques are described in detail in publications by White [11].

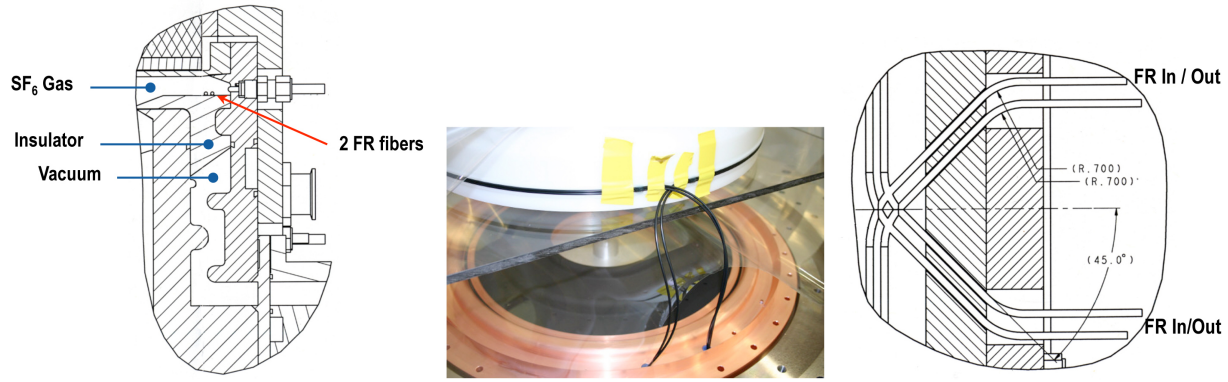

Figure 8. Drawing and photo showing location and routing of Faraday rotation diagnostic fibers. The fibers are mounted on the outside of the HV vacuum insulator.

Figure 9 shows a diagram of a typical layout giving the approximate lengths (in feet) of polarization maintaining fiber, specialty (sensor) fiber, and multimode fiber.

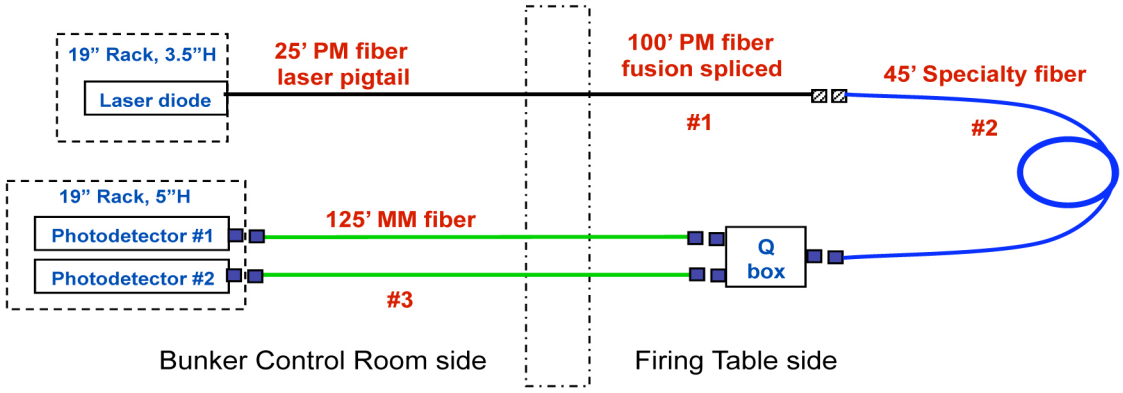

Figure 9. Diagram of basic Faraday rotation diagnostic system.

Free Field B-dot sensors

A three-axis six-loop differential B-dot antenna array is placed approximately ten feet from the generator to monitor leakage flux during the experiment. The height of the array is approximately equal to the height of the transition between the AHG and coaxial generator. The

six loops are arranged in three co-planar pairs. The normal vector of the three co-planar pairs points in the radial, azimuthal, and vertical directions in a cylindrical coordinate system originating at the generator. The loops are made from 3.58-mm semi-rigid coaxial cable formed into 12.7 cm loops. Each co-planar pair consists of two loops of opposite polarity. The two outputs from each co-planar pair are connected via coaxial cable to a balun that strongly attenuates any common-mode signal content. The outputs of the baluns are coupled to the bunker recording digitizers using coaxial cable, within the Faraday cage. The sensitivity of each pair is approximately 13 millivolts per tesla per second. The signal measured by the free field B-dot array can provide information regarding generator performance

SENSOR CALIBRATION

Due to the hand-made nature of our B-dot sensors, the sensitivity varies from probe to probe. The magnitude of this variation has been approximately 5% across the hundred sensors we have made. To minimize the effect of this variation, and to verify probe functionality prior to experiment, we calibrate the sensors.

Calibration of such small insensitive probes is difficult. The mutual inductance that describes coupling from the generator to the B-dot loops is on the order of tens of picohenries. The B-dot probe response is somewhat frequency dependent, due to frequency-dependence in magnetic field structure near the hole through which the B-dot probe is inserted. Time-domain calibration techniques within the bandwidth of interest are quite difficult, due to the large currents necessary to produce signals that can be recorded with adequate resolution on modern recording digitizers. Further, the error introduced by the necessary subsequent integration must be carefully monitored.

Our calibration approach instead uses swept-frequency vector network analyzer (VNA) measurements to achieve the necessary dynamic range [12]. We expand this dynamic range by increasing the amplitude of our measured signals through external amplification, and by minimizing the amplitude of spurious signals by isolating the ground wires of our instrumentation and enclosing it within a Faraday cage.

We perform two independent probe calibrations. The first calibration is performed before the probe is installed in the generator. This calibration is performed in a 50-Ohm coaxial airline calibration fixture. The purpose of this calibration is to verify functionality of the probe. The second calibration is performed after the probes have been installed in the generator, and is used to accurately characterize the *in-situ* probe response. The calibration procedure is similar for both calibrations.

A diagram of the calibration instrumentation is shown in Figure 10. The Agilent 4395A VNA generates a swept-frequency signal between approximately 1 kHz and 250 kHz, which is amplified using an Amplifier Research 350AH1 RF amplifier. The amplifier is capable of driving roughly ten amperes of current into either the shorted airline or coaxial generator. A calibrated current monitor is inserted along this transmission line to monitor the current flowing in this circuit. The output of the current monitor is connected via coaxial cable to VNA port R. The B-dot probe under test, installed in the generator or airline (as shown in Figure 10) is connected with coaxial cable to the VNA port B.

VNA measurement of the B-dot probe output divided by VNA measurement of the current monitor output yields a frequency response for the probe. The ideal frequency response for a time-derivative sensor can be determined from inspection of the Fourier transform pair

$$\frac{df(t)}{dt} \leftrightarrow j\omega F(j\omega) \qquad [1]$$

The output of a B-dot sensor is dependent on the area and number of loops and the orientation of the loops relative to the incident field. These factors can be embodied in a scalar sensitivity $\pm S$ with units volts per ampere per second. The transform pair in Eq. (X) can then be modified accordingly to yield

$$\pm S\frac{dx(t)}{dt} \leftrightarrow \pm Sj\omega X(j\omega) = H(j\omega)X(j\omega) = Y(j\omega) \qquad [2]$$

which states that in the frequency domain, the probe output $Y(j\omega)$ in volts is equal to the frequency response $H(j\omega)$ in units of volts per ampere multiplied by the input signal $X(j\omega)$ in units of amperes. The magnitude of the frequency response $H(j\omega)$ is a line with slope S. The argument of the frequency response $H(j\omega)$ is positive or negative $\pi/2$, with the sign dependent on whether the probe took a positive or negative time-derivative.

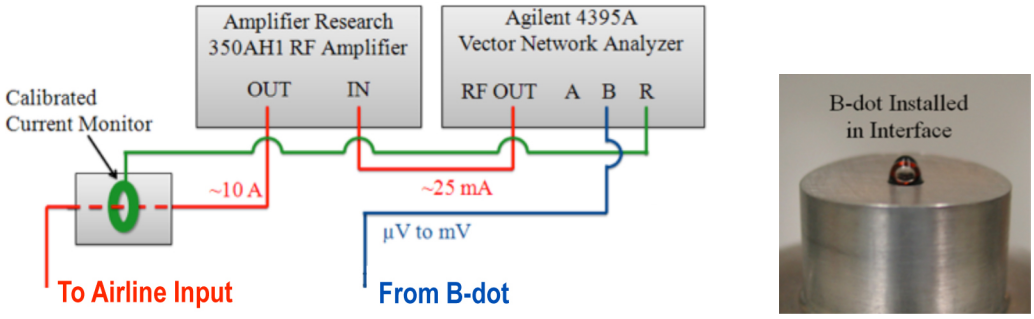

Figure 10. Diagram of VNA setup for sensor calibration in coaxial airline (left). Photo of B-dot sensor holder that mounts flush to inside of airline (right).

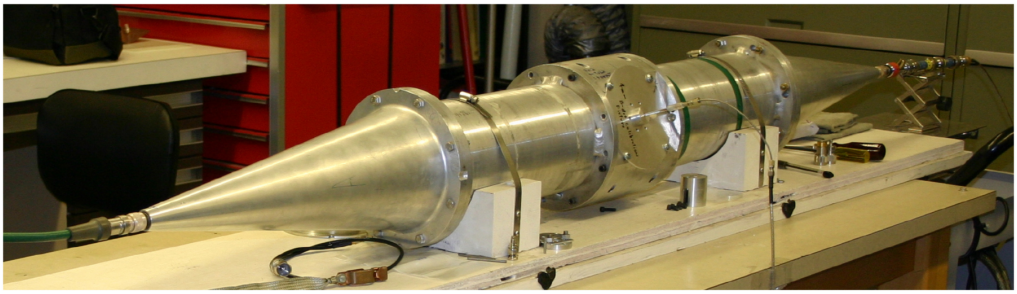

Figure 11. Photo of 6-inch coaxial airline used for sensor calibration. The input end is toward the left. The B-dot holder (Shown in Fig. 10) is inserted in the middle section. The output end (toward right) can be terminated into 50-Ohm or shorted.

We have found that measured frequency responses of our B-dot probes closely resemble the ideal responses. Thus our measurements of VNA port B divided by VNA port R yield a frequency response that is very close to a straight line in the frequency domain. We correct the measured frequency response by removing the CT response, cable response and VNA port response, then use a least-squares fit to the corrected data to determine the probe sensitivity. We observe directly the argument of the frequency response to determine the probe polarity.

FARADAY CAGE APPROACH TO EMI PROTECTION

Our most important pulsed power measurements are at the load end of the coaxial generator. By establishing an experiment ground at this point we were able to create a Faraday cage surrounding the entire pathway where cables carry signals from B-dot sensors directly to digitizers. This is depicted in Figure 12.

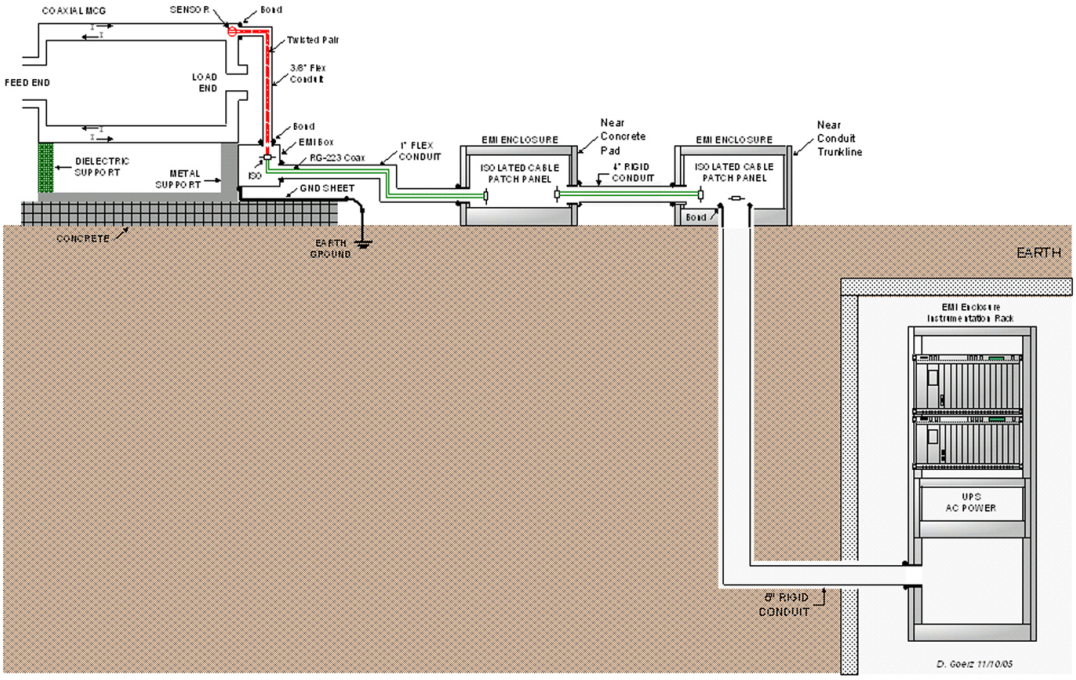

Figure 12. Drawing of output B-dot signal path and EMI shielding (Faraday cage) all the way into bunker. EMI-shielded rack housing digitizers is isolated and energized by an uninterruptable power supply.

The sensors and cables are fully enclosed within EMI-shielded conduits and enclosures all the way to the bunker. All of the conduit connections to EMI enclosures have complete circumferential bonds. For rigid conduits these bonds are welded. Where the trunk-line conduit enters the bunker, connections are made to bunker rebar and outside building ground to provide a wipe-off path for currents flowing along the outside of the conduit. Inside the bunker the rigid conduit is bonded to the EMI-shielded instrumentation rack. This rack has AC power and ground remotely disconnected during the experiment, with instrumentation battery powered by an uninterruptible power supply. The shielding effectiveness of this Faraday cage has been measured, and the results are shown in Figure 13. We regularly measure the attenuation levels provided by the Faraday cage, particularly when configuration of equipment within the bunker has changed. Over the years we have made improvements, like using rigid conduit to the rack, which have provided 20 to 30 dB better shielding effectiveness at the lower frequencies (<10kHz) typical of FCG experiments.

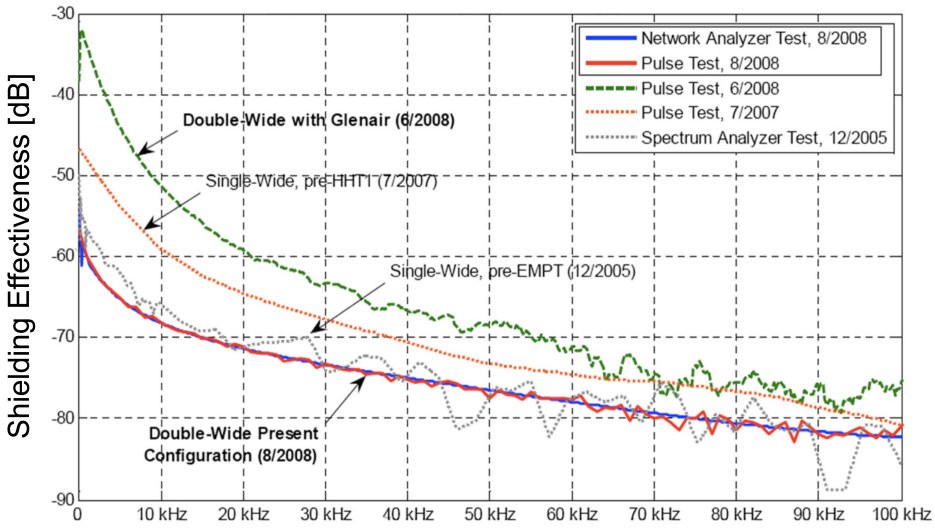

Figure 13. Measured shielding effectiveness of Faraday cage system.

SIGNAL PATH CHARACTERIZATION

The signals generated by our pulsed power sensors are coupled to the bunker via coaxial cable or analog optical fiber links. Within the bunker, the electrical signals are divided with resistive dividers and attenuated as necessary to produce digitized signals that maximize the dynamic range of our recorders.

To increase the accuracy of our recorded signals, we measure the response of the entire data acquisition signal path, and use the measured response to correct the data measured during an experiment. The signal path characterization process consists of three primary measurements: DC loss measurements, VNA swept-frequency characterization, and pulsed timing measurements.

The DC loss measurements are straightforward; a DC voltage is applied at the signal path input, and the voltage at the signal path output is measured. The ratio of the applied voltage to the voltage at the signal path output is the measured DC attenuation for the channel.

The VNA swept-frequency characterization consists of coupling a swept-frequency output through a directional coupler, then into a calibrated cable that is connected to the signal path input. The output of the signal path is connected to the VNA and measured. The output of the directional coupler is measured to provide a reference signal. The ratio between the measure signal path output and the reference signal forms a transfer function for the signal path.

The pulsed timing measurements are performed by measuring the difference in time it takes for a pulse to traverse the signal path as compared with a transmission line of known delay. The measured delay times are used to time-shift data measured during the experiment for comparison on a unified experimental time-scale.

Our VNA transfer function measurements are typically done between 1 kHz and 500 MHz. The low-frequency data is used to compare with the DC loss measurements. The entire transfer function is used to compute the step response for the signal path, which yields both timing and attenuation information. The timing from the VNA step response is limited to one nanosecond resolution, due to the 500 MHz bandwidth of the VNA. The timing from the VNA

step responses and the pulsed timing measurements typically agree to within two nanoseconds, which is less than the time spacing between two samples on our 12-bit recording digitizers.

The DC measurement and low-frequency data from the VNA transfer function measurements typically agree to within a few tenths of a percent. VNA source impedance mismatch accounts for the majority of this error, and can be removed by numerically correcting the transfer function data with measured input impedance data from our signal paths.

The bandwidth of our signal paths is approximately 10 megahertz for analog fiber optic link channels, and approximately 60 megahertz for coaxial cable channels. Since the bandwidth of our measured signals is much lower than this, we have not needed to de-convolve the measured transfer function from our experimental data. We instead scale the measured data by a value determined from the DC loss measurements or low-frequency transfer function information.

Our approach to signal path characterization is guided by a desire for both accuracy and redundancy. By performing several measurements using independent methods and independent instrumentation, we decrease the likelihood of losing or misunderstanding data from hardware that is destroyed during a valuable experiment.

RESULTS

Analyzed data from a full function test of an AHG-CG system is shown in Figure 14.

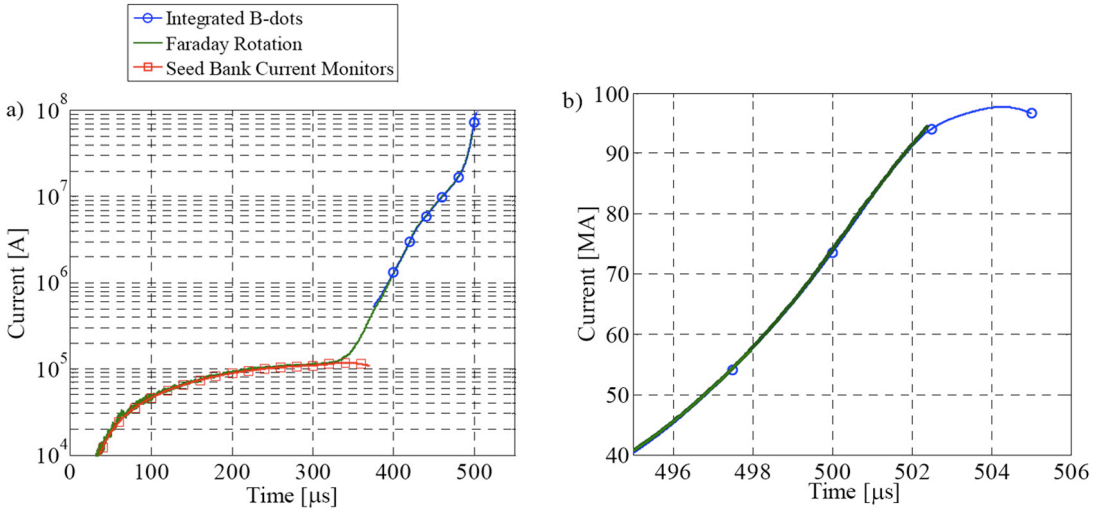

Figure 14. Current waveforms from full function test showing excellent agreement between all measurements.

During operation of the seed bank, current measurements made using CTs in the seed bank, B-dots in the CG, and FR at the output are all in excellent agreement. The Faraday rotation measurement exhibits a tremendous dynamic range (80 dB) from less than 10 kA to nearly 100 MA. The output B-dots, using the Faraday cage EMI shielding, produce high quality data that agrees exceptionally well with the FR measurement, up to the point that the FR fiber failed two microseconds before peak current.

SUMMARY and CONCLUSION

We have developed a family of advanced magnetic flux compression generators used to perform high energy density physics experiments and material science studies. These multistage systems require proper grounding, shielding, and isolation to function properly. In our approach, we establish a single point ground at the load end of the experimental hardware, and all of the pulsed power and diagnostic systems are isolated from ground and each other. Sensors are electrically isolated and signal lines are fully enclosed in metallic conduits to provide EMI shielding. Where necessary, electrical signals are converted to optical signals and carried over fibers. All of the high current sensors are custom fabricated, and we perform in-situ calibration using network analyzer equipment to achieve very accurate characterization. Signals from our output B-dot sensors are carried over coaxial cable to digitizers in the bunker, all within a Faraday cage EMI shield. This provides exceptionally low noise measurements for the most important current measurements.

ACKNOWLEDGEMENTS

This work performed under the auspices of the U.S. Department of Energy by Lawrence Livermore National Laboratory under Contract DE-AC52-07NA27344.

REFERENCES

[1] D. B. Reisman, et al., "The Advanced Helical Generator," Rev. Sci. Instrum. **81**, 034701 (2010).
[2] D. B. Reisman, et al., "The Full Function Test Explosive Generator," Rev. Sci. Instrum. **81**, 036109 (2010).
[3] J. B. Javedani, D. B. Reisman, D. A. Goerz, T. L. Houck, M. P. Perkins, and G. E. Vogtlin, "Application of Modern Modeling and Simulation Codes for Development of Advanced Flux Compression Generators," The 13th International Conference on Megagauss Magnetic Field Generation and Related Topics, Suzhou, China, (2010).
[4] D. A. Goerz, J. B. Javedani, G. E. Vogtlin, T. L. Houck, M. P. Perkins, and D. B. Reisman, "Development of High Performance Vacuum Power Flow Interface for Explosive Magnetic Flux Compression Generator Experiments," The 13th International Conference on Megagauss Magnetic Field Generation and Related Topics, Suzhou, China, (2010).
[5] PPM Ltd, Wiltshire, UK SN6 8TY, http://www.ppm.co.uk
[6] Pearson Electronics, Inc., Palo Alto, CA 94303, http://www.pearsonelectronics.com
[7] North Star Research Corp., Albuquerque, NM 87109, http://www.northstar-research.com
[8] Integrator correction technical note available at website of EG&G, a Division of URS, http://www2.urscorp.com/albuquerque/integrator_correction.htm
[9] Glenair series 74 helical convoluted tubing available from: http://www.glenair.com
[10] L. R. Veeser, G. I. Chandler, and G. W. Day, "Fiber Optic Sensing of Pulsed Currents," Photonics: High Bandwidth Analog Application, Society of Optical Engineering (1986).
[11] A. D. White, G. B. McHale, and D. A. Goerz, "Advances in Optical Fiber-Based Faraday Rotation Diagnostics," 17th IEEE Pulsed Power Conference, Washington, DC, June (2009).
[12] A. D. White, R. A. Anderson, T. J. Ferriera, D. A. Goerz, "Frequency Domain Methods for Characterization of Pulsed Power Diagnostics," The 17th IEEE Pulsed Power Conference, Washington DC, June (2009)